MODELING BEAMFORMERS IN REFRACTIVE MEDIA

David Robert Bergman[1]
[1]Exact Solution Scientific Consulting LLC
3159 Schrader Road, Room 122, 07801, Dover, New Jersey, USA

ABSTRACT

Beamformers are a class of powerful and elegant algorithms for detecting, tracking and imaging sources and targets using phased arrays of sensors. From one point of view the beamformer is sampling the incoming wavefronts at the array face and forming an angle of arrival for these wavefronts. In a homogeneous medium the angle of arrival can be equated to a bearing line that points in the direction of sources or scattering targets. The presence of refractive effects in the propagation media can alter the angle of arrival calculation and cause multiple images even in the absence of boundary reflections. This presentation is divided into three parts: (1) The presentation and discussion of a forward propagation models for modeling the acoustic signals seen (heard) by the phased array, (2) A discussion of systematic effects on beamformer prediction caused by the refractive properties of the environment, and (3) Methods for compensating for these effects to separate the true sources and scatterers from the medium in the beamformer image. We focus attention on modeling these effects in stationary layered media.

1 INTRODUCTION

Phased arrays are used in a variety of applications. Active arrays are used to locate objects based on pulse echo data, while passive arrays are used to locate sources of sound in space [1,2,3]. With the aid of visual data, passive arrays can be used to identify sound sources by associating a peak in detected acoustic power with an object in the space. The beamformer is a signal processing technique that uses array data to locate targets or sources in space [4]. The technique uses relative differences in phase, or arrival time, between members of a group of sensors. The output of these algorithms is a look direction, a vector pointing in the direction of a potential source. When propagating through homogeneous media wavefronts propagate along straight line paths. In the presence of refractive deviations, acoustic signals will tend to propagate along paths that bend toward lower sound speeds and along the direction of fluid flow. This will cause pulses received by an array to be misaligned relative to their expected direction of arrival. In this paper we discuss modeling the beamformer

performance when refractive effects are present in the environment and methods for correcting these effects in the standard beamformer output.

Methods for correcting beamformers or compensating for certain environmental effects are well known. The use of a strong source or sources to measure components of the cross spectral density matrix can be used to correct errors caused by random fluctuation in the propagation media. This method, now well known in acoustic beamformer signal processing, was inspired by a similar technique used in radio astronomy, which uses a bright star as a calibration source for enhancing the signal from weaker stars in the field of view. In this paper we are mainly concerned with the effect of static changes caused by the refractive properties of the environment. In this case refractive changes in the environment cause distortion of ray paths and wavefronts thus violating some of the main assumptions used in the development of beamformer algorithms and analysis of their limits. Due to a theoretical equivalence between the beamformer and a Fourier transform one can think of the beamformer output as an image of the potential sources and/or targets present. The impact of these aberrations on any array of detectors is that whatever data is processed leads to a distorted picture of the source, much like looking through the bottom of a drinking glass and seeing objects in a room morphed to the contours of the glass. This phenomenon and the analysis of its effect on phased array processing derives inspiration from another phenomenon encountered in astrophysics, gravitational lensing. As light travels from distant stars to detectors on or near the earth its propagation path is distorted by the gravitational fields of massive objects. The distorted paths lead to incorrect determinations of potential sources. Some common phenomena associated with this effect are Einstein's Ring and Einstein's Cross, wherein a single point source appears to be a bright ring or sequence of points in a cross formation.

In general relativity light travels along a special class of curves known as null geodesics, curves of zero length in four dimensional space-time. This is also a feature of the bicharacteristics of any hyperbolic partial differential equation. It has been explicitly demonstrated in acoustics that ray paths are in fact null geodesics of a pseudo Riemannian manifold where the metric components of the manifold are related to the local sound speed profile and the wind vector [5,6]. Thus, the phenomenology of gravitational lensing and the types of analysis and corrections employed carry over to the field of acoustics and optics in refractive media (or any other wave propagation governed by a hyperbolic PDE). This machinery has been applied to acoustics to produce generalizations of paraxial ray trace procedure and Gaussian beam equations in the presence of moving fluids with time dependence [7,8,9,10].

The modeling of signal propagation has a twofold purpose. The first is to provide an accurate model of what the array will actually see, a ground truth, for testing the performance of existing beamformers. The second is that these models, if accurate enough, can be used to generate more sophisticated numerical Green's functions for use in a matched field filter should a classic beamformer prove to be too difficult to correct. Thus in this sense a fairly good propagation model is a good investment. This paper investigates three specific topics, (1) the modeling of propagation through a refractive environment, (2) the inclusion of this modeling in standard beamformer performance prediction studies, and (3) the development and application of a model based correction procedure that can help remove environmental effects from a beamformer output. The original abstract mentioned focusing on layered media but we present more general cases with three dimensional refractive volumes as well.

2 THE PROPAGATION MODEL

Several numerical techniques are available for modeling propagation from source to receiver. For dealing with refractive media a dynamic ray trace procedure based on differential geometry was developed. This procedure consists of a 4-dim ray trace, which solves for 3-dim position and travel time, and transport equations that solve for the 2-dim geometric spread along each ray path. A two point boundary value approach is used to find all multipaths between each source receiver pair. Boundary reflections are taken into account by resetting initial conditions for the next step in the procedure, and caustics located by checking for zeros in the geometric cross section. Geometric spread is used to estimate the field amplitude along each ray path and for points close to a caustic a field expansion is used. For completeness the equations used are provided below and the reader is directed to the reference literature for more details [7].

Points in space-time are labeled x^μ, μ = 0,1-3, where μ = 0 is reserved for time, *t*, and indices 1-3 indicate spatial coordinates. Equation (1) is the complete dynamic ray trace procedure in 4-dim. There are 20 degrees of freedom not including constraints. The vectors Y_I, I = 1, 2, measure the geometric spread in two independent directions, $\hat{e}_I^\alpha$, at each point along each ray. The internal basis vectors $\hat{e}_I^\alpha$ are used to define coordinate directions in the tangent plane of the wavefront.

$$\begin{aligned} \dot{x}^\mu &= p^\mu \\ \dot{p}^\mu &= -\Gamma^\mu{}_{\alpha\beta}(x^\nu)\, p^\alpha p^\beta \\ \dot{e}_I^\alpha &= -\Gamma^\alpha{}_{\mu\nu}(x^\beta)\, p^\mu e_I^\nu \\ \dot{Y}_I &= P_I \\ \dot{P}_I &= -\left(R_{\mu\alpha\nu\beta}(x^\sigma)\, p^\alpha p^\beta e_I^\mu e_J^\nu\right) Y_J \end{aligned} \tag{1}$$

The following have been introduced, $g^{\mu\nu}$ ($g^{\mu\alpha} g_{\alpha\nu} = \delta_\nu^\mu$), $\partial_\mu \equiv \partial/\partial x^\mu$, $\dot{X} = dX/d\lambda$, and the Einstein summation convention is used. The effects of the environment are contained in the following quantities. Equation (2) is the Riemann curvature tensor and governs the focusing/defocusing properties of the environment, Eq. (3) is the Christoffel symbol of the second kind and governs the ray path geometry and Eq. (4) is known as the acoustic metric and contains the environmental parameters affecting ray path motion.

$$R^\mu{}_{\alpha\nu\beta} = \partial_\nu \Gamma^\mu{}_{\alpha\beta} - \partial_\beta \Gamma^\mu{}_{\alpha\nu} + \Gamma^\mu{}_{\lambda\nu}\Gamma^\lambda{}_{\alpha\beta} - \Gamma^\mu{}_{\lambda\beta}\Gamma^\lambda{}_{\alpha\nu} \tag{2}$$

$$\Gamma^\mu{}_{\alpha\beta} \equiv \frac{1}{2} g^{\mu\nu}(\partial_\alpha g_{\nu\beta} + \partial_\beta g_{\nu\alpha} - \partial_\nu g_{\alpha\beta}) \tag{3}$$

$$g_{\mu\nu} \equiv \begin{pmatrix} -(c^2 - \upsilon^2) & -\vec{\upsilon}^T \\ -\vec{\upsilon} & id_{3\times 3} \end{pmatrix} \tag{4}$$

Examples of ray traces based on the above are provided in Fig. 1 and Fig. 2. It should be noted that several examples of sound speed and wind profiles exist for which there are exact

solutions to the ray and field equations. These make great toy models for illustrating the effects of the medium on signal propagation. For layered media the full set of dynamic ray trace equations can be integrated to provide a first order set which is equivalent to Snell's law in a moving fluid medium.

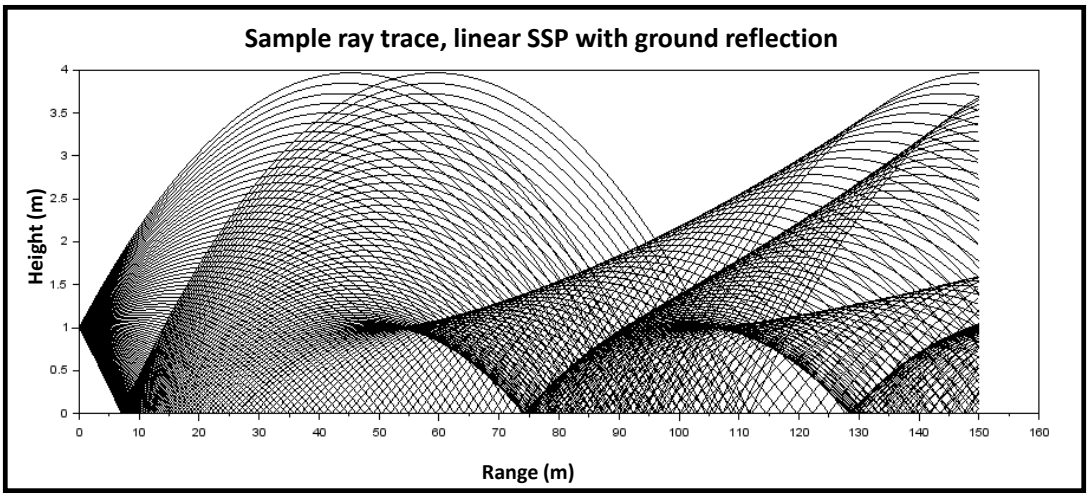

Figure 1. Sample ray trace for a linear sound speed and ground reflection.

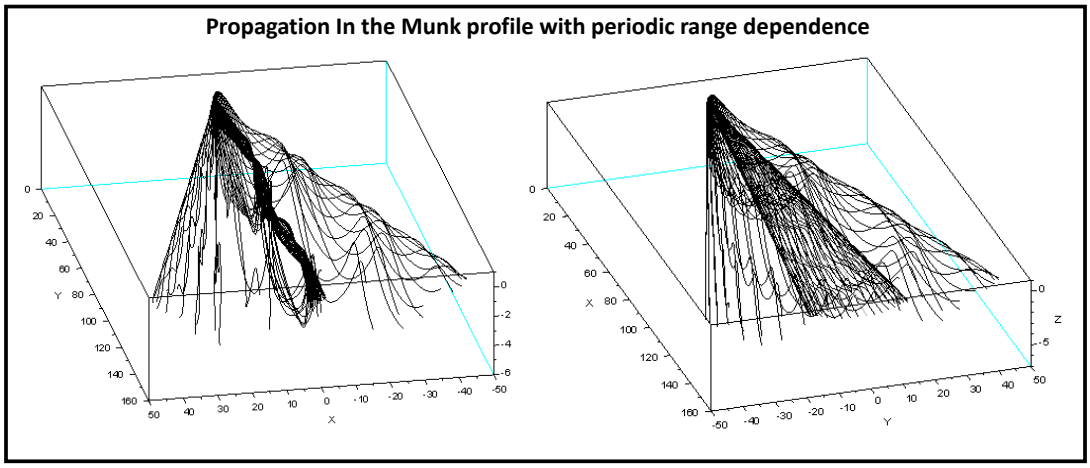

Figure 2. Sample ray trace for in the presence of the Munk profile with periodic range dependence.

3 ARRAY GEOMETRY

The array model consists of a collection of identical sensors distributed in a plane. For the purpose of this presentation we consider each sensor to be ideal, point-like and omni-directional. The inclusion of amplitude response functions depending on frequency and angle of arrival are straight forward but obfuscate the direct relationship between the environment and the beamformer output, which is the primary concern of this paper. Table 1. is a list of basic array geometries and their parameters for modeling purposes.

Table 1. List of array geometries and their parameters

Array Name	Parameters
Line	L, d
Circle	R, d
Rectangle	L_x, L_y, d
Spiral	R_{max}, d
Dougherty Spiral	R_0, v, R_{max}, d
Co-Array	$\vec{r}_i - \vec{r}_j$, $\{\vec{r}_k\}$ are the elements of any existing array.
Random Array	Remove $M < N$ elements from any existing array.

Figure 3. shows samples of several of these arrays. Table 2. lists the parameters used as a description of each subplot in Fig. 1.

Table 2. Modeling parameter for the example arrays in Fig. 1.

Figure 1	Array type	Parameters
(a)	Circle	R = 0.5m, d = 0.05m, N = 63
(b)	Co-Array	Seeded with circle with R = 0.2m, d = 0.05 Total elements N = 1407
(c)	Square	L_x = 1m, L_y = 1m, d = 0.05, N = 441
(d)	Random Array	Starting with the square array in 1 (c) make x = rand(411,1) and map x > 0.5 to T x ≤ 0.5 to F, remove all F elements, N = 217
(e)	Spiral	R_{max} = 0.5m, d = 0.05m, N = 101
(f)	Dougherty Spiral	R_0 = 0.01m, v = 1, R_{max} = 1m, d = 0.05m, N = 32

We treat the array as a set of field points for sampling the propagated signals present in the medium. Several array geometries were looked since it is known that the sensor placement will introduce artifacts into the beamformer output.

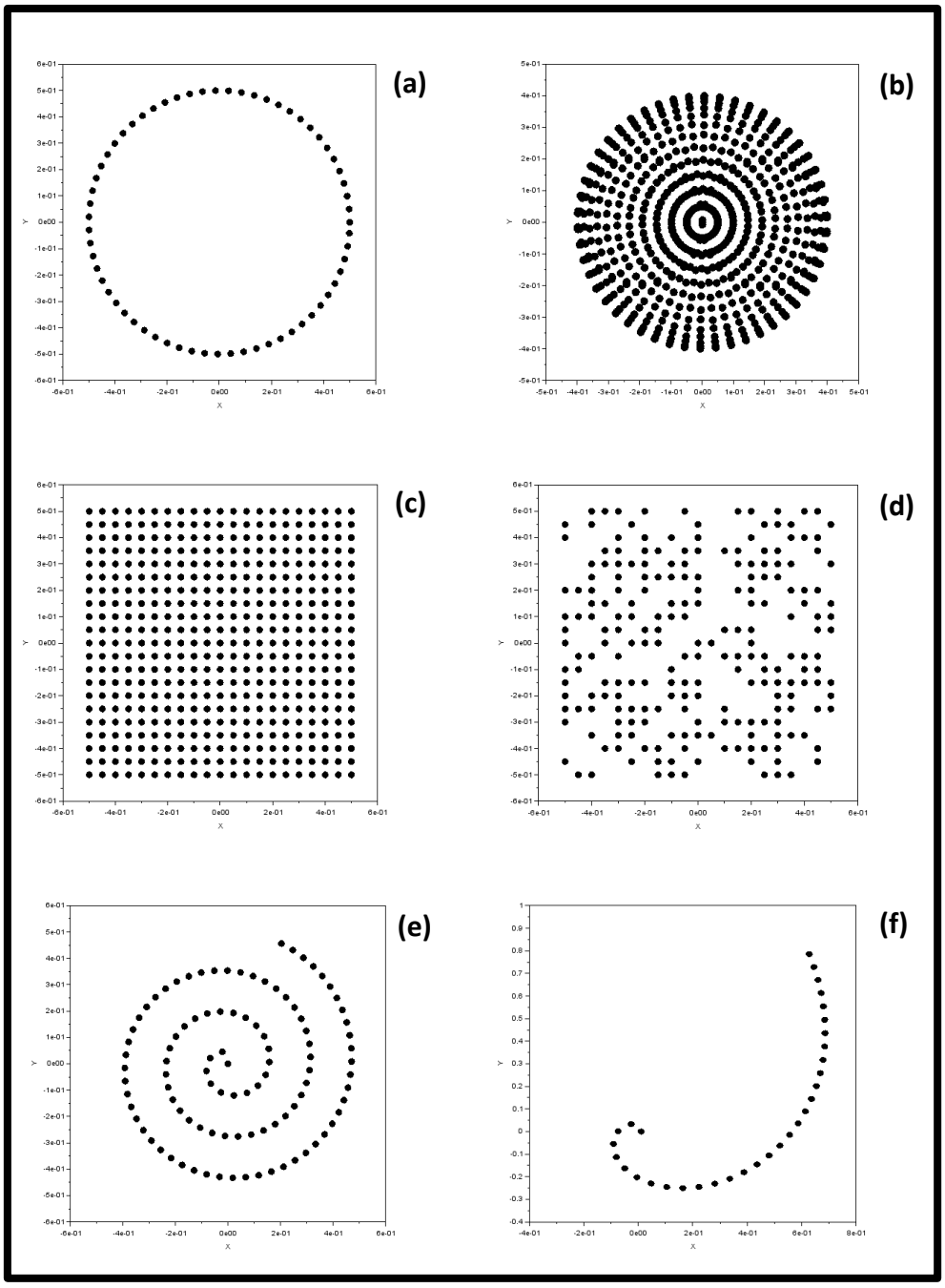

Figure 3. Sample array designs for sampling field data.

4 BEAMFORMER ALGORITHMS

Just as array geometry produces artifacts in the signal processing the specific choice of processing algorithm will affect the output of the array system [11,12,13,14,15]. The starting point for our discussion is the standard delay-and-sum (DAS) beamformer. All processing and field modeling was done in the frequency domain using complex exponentials for beamformer weights, *e.g.* $w_n = \exp(ik_w\hat{k} \cdot \vec{r}_{el})$, where we define the wave number for the carrier frequency, $k_w = 2\pi f/c$, the look direction, $\hat{k}$, and the location of the array elements

relative to the mean sensor location, $\vec{r}_{el}$. The weights were normalized so that $\sum_{n=1}^{N} w_n w_n^{\dagger} = 1$.

$$b(\hat{k}) = \sum_{n,m=1}^{N} w_n^{\dagger} S_{nm} w_m \tag{5}$$

In Eq. (5) the matrix *S* is the cross spectral density matrix formed by taking correlations between all pairs of array element signals. The beam pattern is evaluated on a grid of values (referred to here as a scan grid) that sample the look direction, $\hat{k}$. The beam dependence on look direction comes from the weights and each value can be interpreted as the likelihood that energy is incident on the array from direction $\hat{k}$. The scan-grid is defined with the center of the grid on the equator of a sphere with the array placed at the center of the sphere, appropriate far field assumptions being made. The beam power pattern is then truncated by a minimum desired signal threshold and the resulting data scanned for peaks, local maxima, using interpolated data to locate true maxima more accurately. The angular coordinates of each peak, (θ_j, φ_j), are then taken to be the bearing of a detected signal.

It is fairly easy to interpret what a DAS beamformer is doing. The weighting functions can be thought of as a basis set for a function space, similar to a Hilbert space in quantum mechanics or a mode expansion. When the array data is passed through the beam former algorithm it is essentially measuring how much the data is similar each basis function. Properly normalized the strength of the peak in a beamformer output can be interpreted as the likelihood that the data matches a particular basis function. When pure phases are used as weights the data is decomposed into plane waves coming from infinity. For targets that meet the far field approximation relative to the array a maximum value for a given basis may be interpreted as evidence that there is a source at that look direction. For an active array the time to detect a return of a pulse would indicate target range. Table 3. below lists the other beamformer algorithms investigated in this study.

Table 3. Beamformer algorithms considered in this paper

List of beamformer algorithms investigated
Delay and Sum (DAS)
Maximum Likelihood Method (MLM)
Maximum Entropy Method (MEM)

In Fig. 4 we present examples of the DAS beamformer for three different array geometries. Figure 5 illustrates the difference between the DAS and MEM beamformers for three sources in a motionless environment with a constant sound speed.

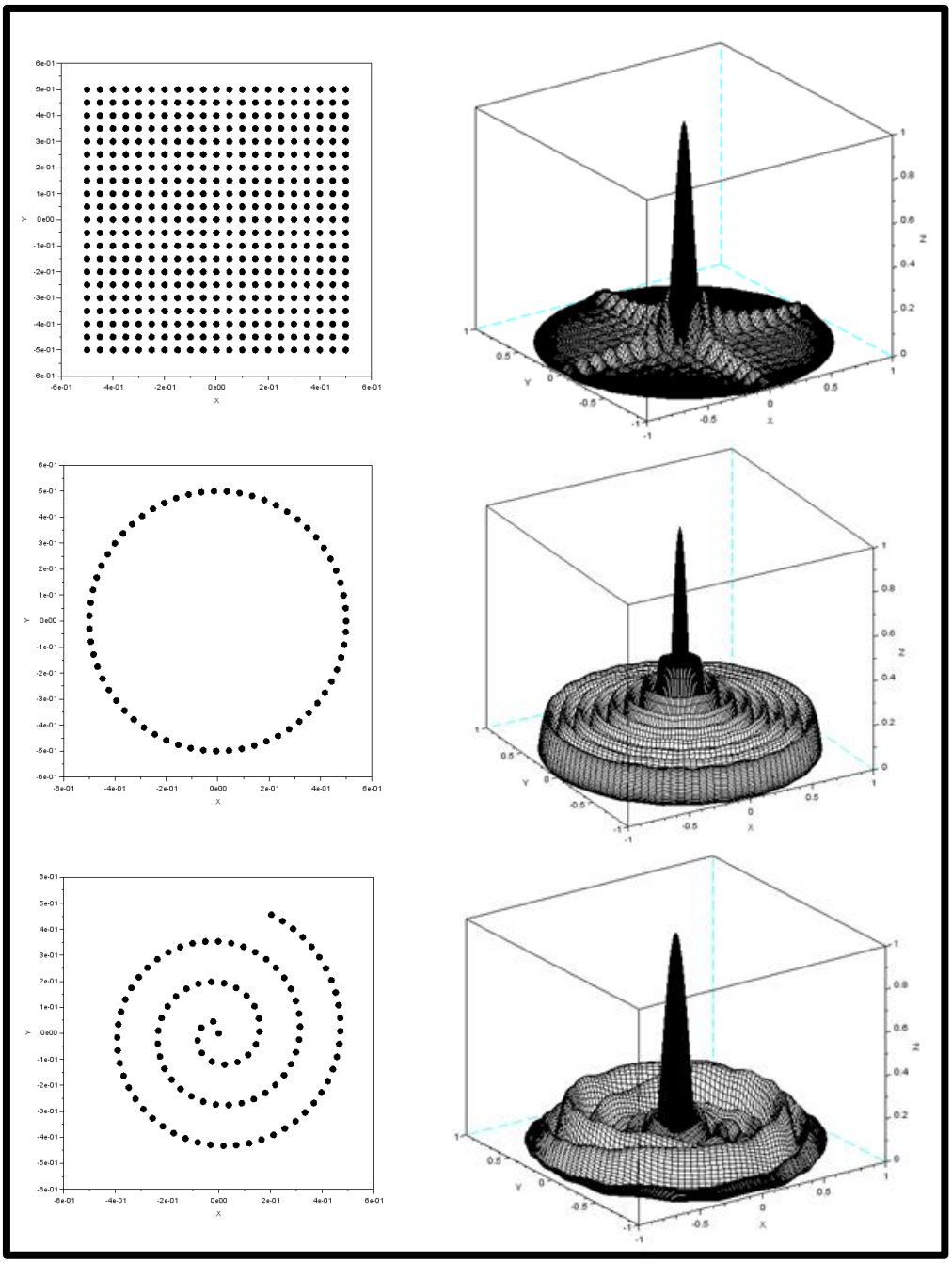

Figure 4. Samples of Beamformer patterns for a square (top), circular (middle) and spiral (bottom) array for a frequency of 3kHz.

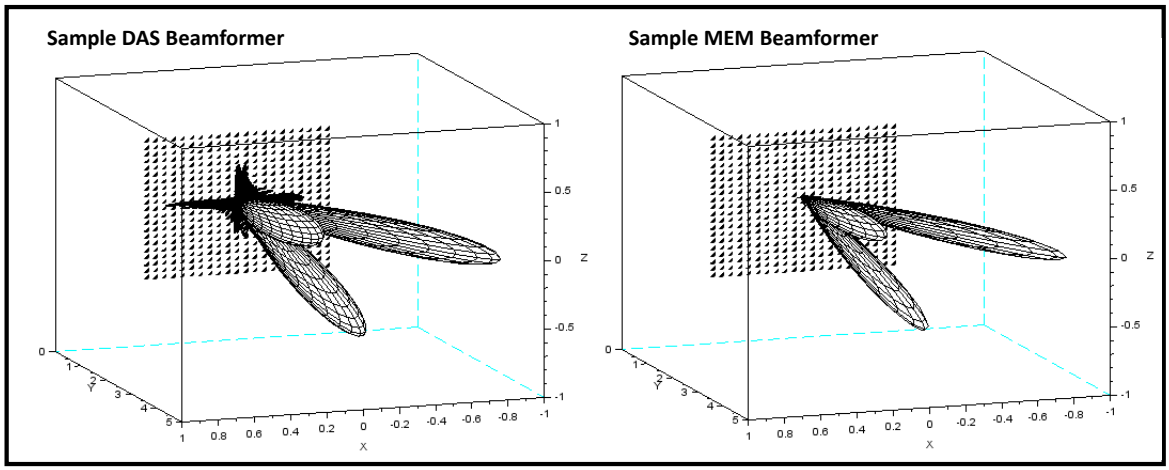

Figure 5. Example of DAS and MEM beamformer outputs plotted relative to the array face. In each case three sources are present.

5 PERFORMANCE PREDICTION

An example of the end to end simulation is provided in Fig. 6. The beamformer along with appropriate signal location and windowing functions provides the front end of a more sophisticated signal processing chain. From the beamformer output we apply a signal threshold and peak finder algorithm. This is designed to locate individual bearing lines which are likely to correlate to a source or target. Figure 6 presents a view of the complete end to end model showing source, array, propagation of the field, resulting beamformer output and bearing line calculation.

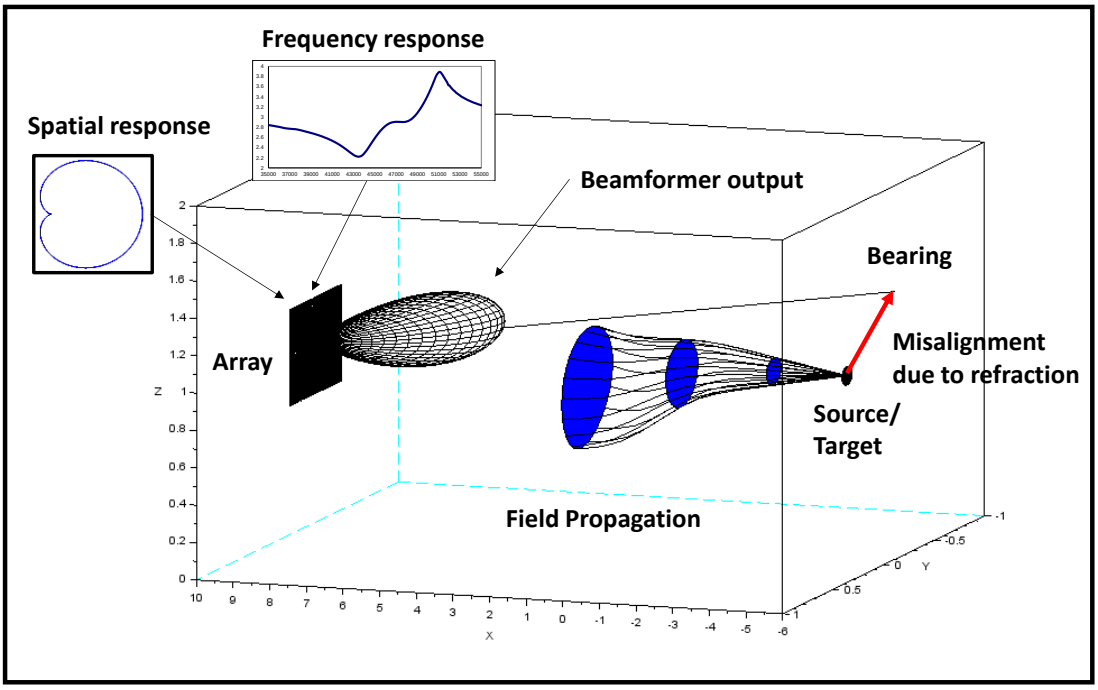

Figure 6. End to end simulation of source location using a phased array.

In a flat motionless environment the beamformer will locate a source or sources provided that they can be resolved for the frequency and array parameters of the system and aliasing does not occur. In the presence of refractive effects array bearings cannot be expected to align with sources or targets [15]. Figure 7 and Figure 8 illustrate these effects for a linear SSP with and without ground reflection.

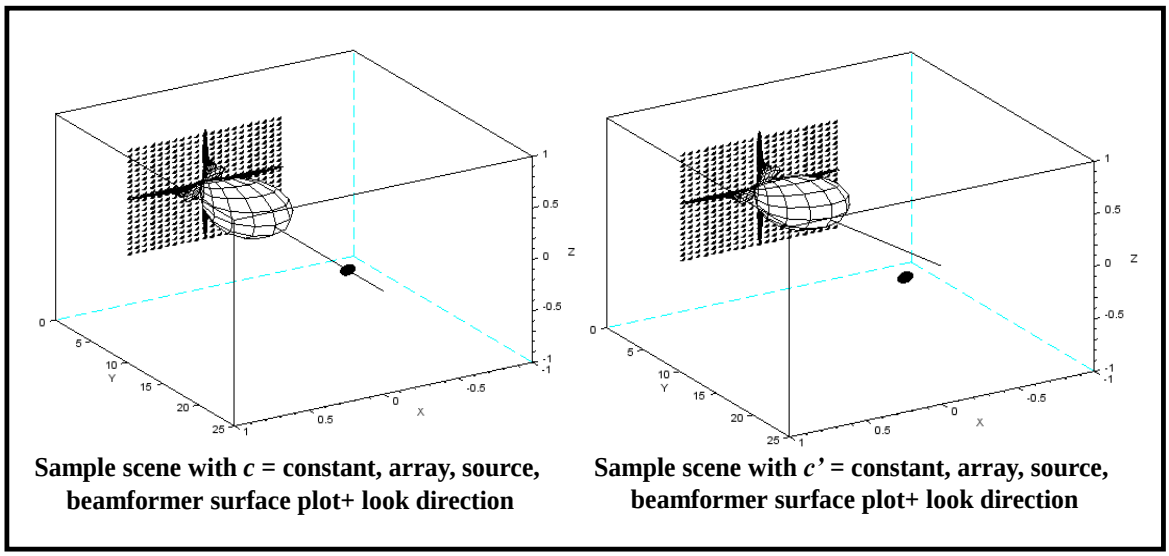

Figure 7. Example of beamformer output and bearing for a source in a flat environment (left) and in the presence of a linear SSP (right).

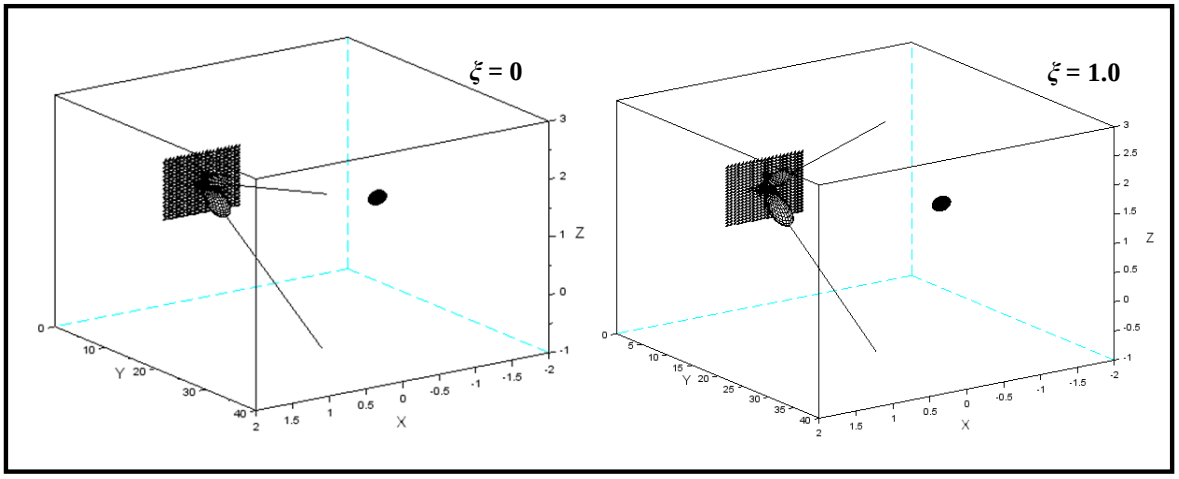

Figure 8. Similar to the case presented in Fig. 7 with the addition of a hard ground reflection at z = 0.

6 IMAGE CORRECTION AND THE THIN LENS EQUATION

The lensing equation relates the observed bearing (or angle of arrival) to the straight line path from source to receiver [16,17]. This is a deceptively simple looking equation. Figure 9 illustrates the parameters in the equation.

$$\boldsymbol{\beta} = \boldsymbol{\theta} - \frac{D_{ds}}{D_s}\hat{\boldsymbol{\alpha}}(\boldsymbol{\xi}) \tag{6}$$

In Eq. (6), $\boldsymbol{\beta}$ is the unperturbed angle of arrival, $\boldsymbol{\theta}$ is the observed angle (with environmental effects factored in) and the last term contains all the refractive properties of the environment in the term $\hat{\boldsymbol{\alpha}}(\boldsymbol{\xi})$. The lensing factor depends on the transverse deflection parameter, $\boldsymbol{\xi} = D_d\boldsymbol{\theta}$. The deflection term is determined by the local sound speed and wind vector integrated along the ray path. Hence direct application of this equation is challenging. We are concerned with two cases: 1) when a propagation path contains finite, bound regions causing deflection and 2) when the refractive effect is weak over the total distance from source to receiver.

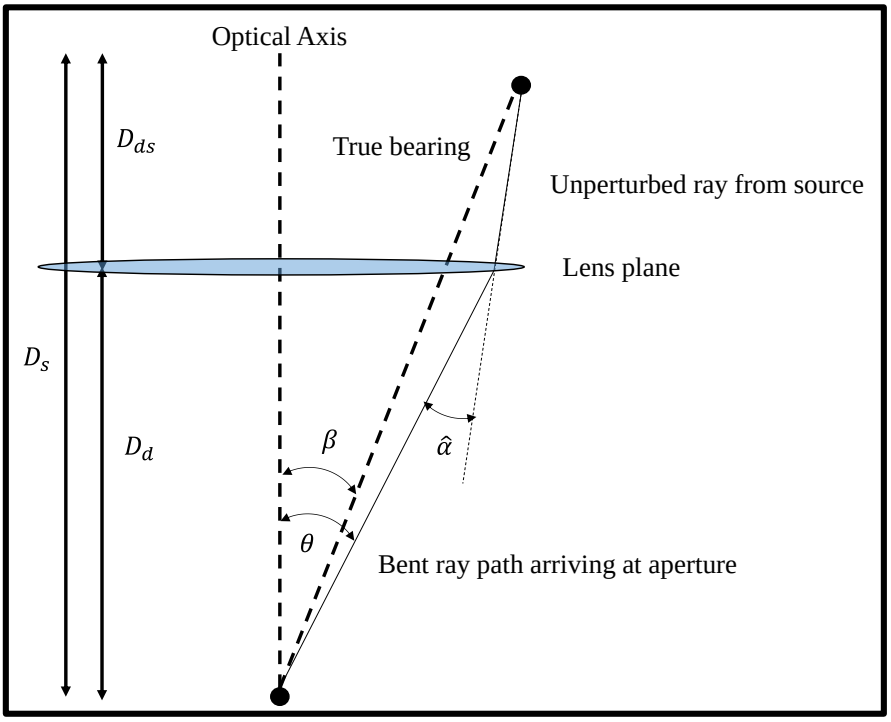

Figure 9. Definition of lens equation parameters.

The lensing factor can be related to the local properties of the medium. Starting from the ray equation, in a suitable representation, the lensing angle is defined as the integral of $d\hat{t}/ds$ along the ray path. Hence, by definition $\hat{\boldsymbol{\alpha}}(\boldsymbol{\xi}) = \Delta\hat{t}$. This illustrates the use of the approximation that the rays be near the optical axis. In this representation the tangent vector, $\hat{t}$, is a unit vector in 3-dim. From the ray equation we have the following expression for the lens angle.

$$\hat{\boldsymbol{\alpha}}(\boldsymbol{\xi}) = \int \vec{\nabla}_{\perp}\varphi dl + \int \hat{t} \times (\vec{\nabla} \times \psi\vec{w}) dl \tag{7}$$

In Eq. (7) we introduce the operator $\vec{\nabla}_{\perp} \equiv \vec{\nabla} - \hat{t}(\hat{t} \cdot \vec{\nabla})$ and define the following scalars, and c_0 is a reference sound speed.

$$\varphi = -\frac{c_0^2 - c_r^2 + w^2}{c_0^2 + c_r^2 - w^2}$$

$$\psi = \frac{2c_0}{c_0^2 + c_r^2 - w^2}$$

Starting from the definition of the deflection angle and the potential functions we work out the deflection explicitly as a function of the environmental fields. The gradient of the potentials is,

$$\vec{\nabla}\varphi = -c_0\vec{\nabla}\psi = \frac{4c_0^2\left(c_r\vec{\nabla}c_r - w_k\vec{\nabla}w_k\right)}{(c_0^2 + c_r^2 - w^2)^2}.$$

Continuing the derivation in the general case is not very illuminating. However we may apply some approximations that are valid in many real life situations. The first will be that the local sound speed is described by $c_r = c_0(1 + \varepsilon f(\vec{r}))$, with $\varepsilon \ll 1$. The second assumption is that the local wind speed is small compared to the sound speed, *i.e.* low Mach number. Since deviations in local sound speed are small we define the Mach number relative to the reference sound speed, $\vec{M} = \vec{w}/c_0$. Now we focus on expanding the potential gradient in powers of ε and *M*.

$$\vec{\nabla}\varphi = \frac{4\left((1+\varepsilon f)\varepsilon\vec{\nabla}f - M_k\vec{\nabla}M_k\right)}{(1 + (1+\varepsilon f)^2 - M^2)^2} \approx (1-\varepsilon f)\varepsilon\vec{\nabla}f - M_k\vec{\nabla}M_k \tag{8}$$

In Eq. (8) we have retained only terms up to second order in the small quantities, ε and $\vec{M}$, dropping terms such as εM^2, $\varepsilon^2 M$ and M^3 etc., and the summation over *k* is implied. In general we do not consider the gradient of small quantities to be of the same order of smallness. However, under the assumption that derivatives of small quantities are likewise small we see that to lowest order $\vec{\nabla}\varphi \approx \varepsilon\vec{\nabla}f$. Applying the same approximations to the second integral and keeping only first order terms in small quantities leads to only one surviving term, $\hat{t} \times \left(\vec{\nabla} \times \vec{M}\right)$.

$$\hat{\boldsymbol{\alpha}}^{(1)}(\boldsymbol{\xi}) = \varepsilon \int \vec{\nabla}_\perp f dl + \int \hat{t} \times (\vec{\nabla} \times \vec{M}) dl \tag{9}$$

Second order effects can be worked out, and are provided below.

$$\hat{\boldsymbol{\alpha}}^{(2)}(\boldsymbol{\xi}) = -\varepsilon^2 \int f\vec{\nabla}_\perp f dl - \int M_k\vec{\nabla}_\perp M_k dl - \varepsilon \int \hat{t} \times (\vec{\nabla} \times f\vec{M}) dl \tag{10}$$

We present these terms to make the point that the wind effects will couple to the sound speed, as is well known from a study of the paraxial ray equations. For weak environmental effects the wind and sound speed effects can be approximately considered additive. This makes the application of the lens equation very simple. Finally we note that for a layered

media, $c(\vec{r}) = c_0(1 + \varepsilon f(z))$, $\vec{\nabla}_\perp \varphi \approx \varepsilon f'(z)\hat{k}_\perp$ to lowest order. It should be noted that this expression generalizes for a layered media in direction $\hat{d}$ by replacing $\hat{k}$ with $\hat{d}$ and *z* with the appropriate linear combination of Cartesian coordinates. The full deflection angle is calculated by integrating along the unperturbed path with an orthogonal impact vector added, *i.e.* by evaluating the integrand $\vec{r} = l\hat{t} + \vec{\xi}$, $\hat{t} \cdot \vec{\xi} = 0$ and integrating along *l*.

We looked at several model environments. Some are reasonable representations of physical situations while other are more of thought experiments designed to illustrate the use of the lens map for correcting array output. These are listed below.

Table 4. Model environments

Description	Profile functions	Eqn. No.
Linear SSP	$c = c_0(1 + \varepsilon z)$	(11)
Step function	$c = c_0 + c_1 u(-\sigma z)$	(12)
Gaussian refraction	$c = c_0\left(1 + \sum_{n=1}^{N} \varepsilon_n \, exp\left(-\frac{(\vec{r} - \vec{r}_0)^2}{2\sigma_n^2}\right)\right)$	(13)
Laminar wind region	$\vec{w} = w_y(z)u(\sigma x)u(-\sigma(x - x_0))$	(14)

The step function, *u*, is defined as $u(\sigma x) = 0.5(1 + \tanh(\sigma x))$, and approaches a jump discontinuity as $\sigma \to \infty$. For these choices the lens correction factor can be evaluated by hand as a function of $\vec{\xi}$, usually in closed form involving special functions.

7 DISCUSSION

The complete beamformer output contains artefacts from the array geometry and signal processing choices that are not the result of propagation. Applying the lens correction to the entire beamformer output would morph these features unnaturally. Applying the lens correction to the bearing angles provides good results for aligning the acoustic bearing with a sound source. The procedure works for multiple sources when they can be resolved by the array and are not too close to endfire. It should be noted that the lens correction can be extended to multiple refractive obstacles by applying the procedure recursively from one lens plane to the next treating the output on one lens and the source or input to the next. This was investigated in simulated experiments using Eq. (13) with several refractive pockets.

In contrast to a full matched field filter the lens approach allows one to use the standard free space Green's function or pure phase in a classic beamformer and apply a reasonable correction to the output. While this presentation focused on modelling and simulation the author has used this technique in active phased array processing. For such applications metrology equipment was deployed in the test facility and interfaced with the array processing unit.

REFERENCES

[1] William S. Burdic. "Underwater Acoustic System Analysis." Prentice-Hall, New Jersey, 1984.

[2] M. Skolnik. "Radar Handbook Second Edition." McGraw Hill, 1990.

[3] Thomas J. Mueller (Ed.), Aeroacoustic Measurements, Springer 2002.

[4] Robert P. Dougherty. "What is Beamforming?" BeBeC-2008-01, 2nd Berlin Beamforming Conference, 2008.

[5] W. Unruh. "Experimental black home evaporation?" Phys. Rev. Lett., **46**, 1352-1353, 1981.

[6] R. White. "Acoustic ray tracing in moving inhomogeneous fluids." J. Acoust. Soc. Am., Vol. 53, No. 6, 1700, 1973.

[7] D. R. Bergman. "Generalized space-time paraxial acoustic ray tracing." Waves in Random and Complex Media, Volume 15 Issue 4, 417 – 435, 2005.

[8] D. R. Bergman. "Symmetry and Snell's Law.", J. Acoust. Soc. Am. **118**, 1278, 2005.

[9] D. R. Bergman. "Internal symmetry in acoustical ray theory." Wave Motion, Volume 43, Issue 6, 508 – 516, 2006.

[10] D. R. Bergman. "Differential Geometry and Ray Theory.", International Journal of Sound and Vibration, ICSV22 conference proceedings, 2015.

[11] R. F. Gragg. "High-Resolution Beamforming in Shallow Water." NRL Report 9143, Naval Research Laboratory Washington D.C., 1989.

[12] S. Stergiopoulos, A. Dhanantwari. "Advanced beamformers for 3D ultrasound systems deploying linear and planar phased array probes." Defense Research and Development Canada, Technical Report TR 2002-058, May 2002.

[13] Z. Wang *et al*. "Constant-beamwidth and constant-powerwidth wideband robust Capon beamformers for acoustic imaging." J. Acoust. Soc. Am. **116** (3), September 2004.

[14] D. B. Ward, R. A. Kennedy, R. C. Williamson. "Theory and design of broadband sensor arrays with frequency invariant far-field beam patterns." J. Acoust. Soc. Am. **97** (2), February 1995.

[15] D. R. Bergman. "Beamformer Performance in Variable Environments", Proceedings SPIE.DSS, Ground/Air Multisensor Interoperability, Integration, and Networking for Persistent ISR VI, 94640X, 2015.

[16] P. Schneider, J. Ehlers, E. E. Falco. "Gravitational Lenses." Astronomy and Astrophysics Library, Springer-Verlag, 1992.

[17] Volker Perlick. "Ray Optics, Fermat's Principle, and Applications to General Relativity." Springer, Berlin, 2000.